Evolution of a fractal system with conserved order parameter under thermal annealing

2010 J. Phys.: Condens. Matter 22 195107

(http://iopscience.iop.org/0953-8984/22/19/195107)

IOP Publishing Journal of Physics: Condensed Matter

J. Phys.: Condens. Matter **22** (2010) 195107 (7pp) doi:10.1088/0953-8984/22/19/195107

Evolution of a fractal system with conserved order parameter under thermal annealing

J Bahadur[1,3], S Mazumder[1], D Sen[1] and S Ramanathan[2]

[1] Solid State Physics Division, Bhabha Atomic Research Centre, Trombay, Mumbai-400085, India

[2] Materials Science Division, Bhabha Atomic Research Centre, Trombay, Mumbai-400085, India

E-mail: jbahadur@barc.gov.in

Received 4 January 2010, in final form 23 March 2010

Published 23 April 2010

Online at stacks.iop.org/JPhysCM/22/195107

Abstract

Mesoscopic structural evolution under thermal annealing of yttrium aluminium garnet fractal aggregates has been investigated by small-angle neutron scattering. Fractal dimension remains invariant with sintering temperature but the extent of the fractal realm is narrowed down significantly. A Monte Carlo simulation, based on Ostwald-ripening type of relaxation of fractal aggregates for a mass conserved system, has been attempted in order to understand the aforementioned novel observation. A local group merge sintering model was adopted for the relaxation of the fractal aggregates. Diffusion driven mass transport over local branches of fractal clusters causes smoothening of branches but keeps the overall shape unaltered at lower resolution. Predictions of the model were found to be consistent, in terms of microstructural evolution, with experimental data. The present simulation was also successful in explaining the evolution of the particle size distribution of the aggregate. To the best of our knowledge this is the first reported experimental and theoretical investigation on the effect of annealing temperature on nano-ceramic fractal aggregates.

(Some figures in this article are in colour only in the electronic version)

1. Introduction

The formation, evolution and consequences of instabilities in materials have been the subject of intense investigation in the last two decades [1–6]. Instabilities during growth, evolution and construction of systems with non-equilibrium morphologies that imitate the spontaneous pattern formation in nature, play an important role in physics, chemistry, materials science and biology [7–9]. Such investigations provide insights into fundamental issues pertaining to the interplay and balance governing the bulk and surface contributions to the energetics of materials, their morphological stability and relaxation dynamics in non-equilibrium complex systems.

In general, precipitation and sol–gel synthesis methods are widely used to prepare nano-ceramic powders. The growth of nano-particle aggregates may result in unstable dendrite structures with a large surface to volume ratio depending on the thermodynamical environments [10]. The concept of fractal geometry is widely used to describe such spatially inhomogeneous systems [11–13].

However, although growth mechanisms for fractal structures have been studied extensively, subsequent structural relaxation after growth remains an important issue from the physics point of view. It is worth mentioning that a fractal cluster is thermodynamically metastable [14] as the ratio of its surface to volume is significantly large. Therefore, it is of fundamental importance to analyse possible pathways of relaxation processes towards more stable configurations with respect to some thermodynamical variable. The excess surface energy of fractal objects gives rise to a number of evolutionary processes that lead to significant structural modifications during their relaxation [15–19]. Pertinent physical examples include [15–19] annealing of dendrite inclusions in solids,

[3] Author to whom any correspondence should be addressed.

healing of cracks in ceramics during sintering, temperature-induced transformations in composites, relaxation of rough surfaces, ageing of colloidal particles, etc. In all the above cases, the total amount of mass remains conserved during the evolution which is driven by the excess interfacial energy.

There are two broad types of restructuring [20] of fractal clusters during sintering. In the first case, fractal aggregates of weakly bonded primary particles tend to collapse and become more compact during annealing [21, 22]. In the second case, fractal aggregates of strongly bonded particles retain their general topology with a decrease in the radius of gyration and an increase of size of the subunits due to sintering at high temperatures [23, 24]. In recent studies [25–27], simulations for thermal annealing of 2D fractals have been carried out, where coarsening of their arms is taken as the dominant mechanism for their shape relaxation. In such a coarsening type of relaxation, restructuring occurs when neighbouring particles form bonds and merge in order to reduce their surface energy and approach a more favourable thermodynamical state [28–33]. A coarsening of the fractal cluster exhibits a scaling phenomenon, i.e. a morphological pattern of the domains at an earlier time looks statistically similar to a pattern at a later time apart from the global change of scale implied by the growth of a characteristic length scale [34–38].

In a structural relaxation of fractals during sintering, two major parameters that govern the evolution are temperature and time. Considering a linear sintering law for two spherical particles in terms of the total surface area reduction, we can write a $\frac{da}{dt} = -\frac{(a-a_s)}{\tau_f}$, where a_s is the final surface area of coalesced particle with conserved volume and τ_f is the characteristic sintering time [29, 39, 40]. It is evident from above equation that the evolution under sintering depends on the characteristic sintering time τ_f [41], which is given by $\tau_f = A d_p^4 \exp(\frac{E_a}{kT})$, where A is the pre-exponent factor, E_a is the activation energy of the diffusion process, k is the Boltzmann constant, T represents the temperature and d_p is the diameter of individual particle. An increase in temperature results in an enhancement of the mobility of the cluster atoms leading to faster sintering kinetics.

It is important to note that, although extensive investigations [14–33] have been performed on temporal relaxation of fractal cluster, structural relaxation as a function of temperature is yet to be reported. Furthermore, earlier investigations dealt with restructuring of fractal clusters with monodisperse constituent particles. However, in general, if the constituent particles in an aggregate possess polydispersity in their size, the model for the sintering of the fractal cluster becomes more complex.

The present investigation is a step towards understanding the effect of sintering temperature on the fractal cluster and the effect of mobility of the primary particle on the fractal cluster. Small-angle neutron scattering experiments have been performed on yttrium aluminium garnet (YAG $\cong$ $Y_3Al_5O_{12}$) nano-ceramics synthesized by a precipitation route as a function of sintering temperature with fixed sintering time. Interestingly, it has been found that coarsening of fractal aggregates occurs due to sintering but the fractal dimension remains invariant for a wide range of temperature. To understand such a novel experimental observation, a computer simulation has been carried out. The computer simulation deals with the evolution of morphological changes of a 2D diffusion limited aggregate (DLA) structure. To the best of our knowledge, this is the first reported investigation on the effect of sintering temperature on nano-ceramic fractal aggregates.

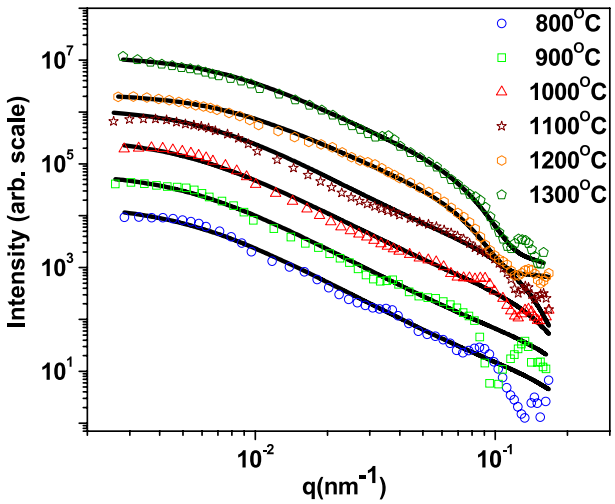

Figure 1. SANS profiles on a log–log scale for specimens sintered at different temperatures. Solid line represents the fit of the model to the scattering data. The profiles are shifted vertically for clarity.

2. Experiments

A precursor for YAG has been prepared by a homogeneous precipitation technique using an aqueous solution of aluminium nitrate, yttrium nitrate and urea with molar concentrations of Al^{3+}:Y^{3+}:urea as 0.2:0.12:1.4. The solution of the mixture was thermostated at 95 °C for 3 h for completion of precipitation. The precipitate thus formed was filtered, washed repeatedly (thrice) with distilled water followed by final washing with acetone. The wet cake thus formed was dried in an air oven overnight and was decomposed at 850 °C to form a phase of pure YAG powder which we call the as formed or virgin powder. The resulting YAG nano-ceramic powder possesses an aggregated structure [42]. The as formed powder was sintered at 800, 900, 1000, 1100, 1200 and 1300 °C, respectively.

Small-angle neutron scattering (SANS) [43, 44a, 45, 46] experiments were carried out using a double crystal based medium resolution small-angle neutron scattering instrument (MSANS) [47] at the Guide Tube Laboratory of the Dhruva rector at Trombay, India. The scattered intensities were recorded as a function of wavevector transfer q ($=4\pi \sin(\theta)/\lambda$, where 2θ is the scattering angle and λ ($=0.312$ nm) is the incident neutron wavelength for the present experiment). Measurements were performed on YAG specimens sintered at different temperatures. SANS profiles were recorded in the q-range $\sim$0.003–0.17 nm^{-1}. SANS profiles of the specimens were corrected for transmission and instrument resolution [48] prior to further analysis. The corrected profiles are shown in figure 1.

3. SANS data analysis

From figure 1, it is evident that the scattering profiles show a linear domain over a wide q-range when plotted on a double logarithmic scale. The extent of the linear domain varies with sintering temperature while the slope of the linear region remains invariant for all profiles. In view of the above fact, scattering profiles have been analysed by assuming a fractal type correlation of the primary nano-particles of the specimens. In such a case, the scattered intensity [44a] may be represented as

$$I(q) = C\left[\int D(r)V^2(r)P(q,r)\,\mathrm{d}r\right]S(q,r_{\mathrm{av}}), \qquad (1)$$

where $P(q,r)$ is the spherical form factor for primary nano-particles, $V(r)$ is volume of a particle of radius r and C is q independent scale factor. The spherical form factor is valid at various sintering temperatures, as explained below. Sintering is a process to consolidate the aggregates by the coalescence of the primary particles into bigger particles leading to a smaller surface to volume ratio. It is interesting to note that sintering at fixed temperature involves three different stages [44b]. During the initial and intermediate stages of sintering, the shape of the coalesced particles may be different as compared to the spherical one. However, in the final stage of the sintering the coalesced particles formed by merging of the initial spherical particles will be spherical as the surface to volume ratio will be the smallest as compared to that for other shapes. In the present study, scattering measurements were performed for different sintering temperatures in the final stage of sintering, i.e. we are dealing with aggregates at the final stage of sintering where the constituent coalesced particles remain spherical ones. Thus, it is justifiable to take the spherical form factor in equation (1) for different sintering temperatures.

Furthermore, the primary particles are always polydisperse in nature with a variation in degree of polydispersity. In the present case, a normalized log-normal distribution,

$$D(r) = \frac{1}{\sqrt{2\pi\sigma^2 r^2}}\exp\left[-\frac{[\ln(r/r_0)]^2}{2\sigma^2}\right],$$

is assumed as the size distribution of the primary particles of the aggregates, where r_0 and σ (polydispersity index related to width of the distribution) are the two parameters of the distribution and related to the mean radius, $r_{\mathrm{av}} = r_0\exp(\sigma^2/2)$. The distribution of a variable is modelled as log-normal when the distribution is generated by many multiplicative effects [46, 49]. In equation (1), $S(q,r_{\mathrm{av}})$ represents the structure factor, due to fractal correlation of the particles [50, 51] in the aggregate and is given by

$$S(q,r_{\mathrm{av}}) = 1 + \frac{1}{(qr_{\mathrm{av}})^{D_{\mathrm{F}}}}\frac{D_{\mathrm{F}}\Gamma(D_{\mathrm{F}}-1)}{\left[1+\frac{1}{q^2\xi^2}\right]^{(D_{\mathrm{F}}-1)/2}} \times \sin[(D_{\mathrm{F}}-1)\tan^{-1}(q\xi)], \qquad (2)$$

where D_{F} is the fractal dimension, r_{av} is the average size of the primary particles forming the aggregate and is assumed as the lower cutoff of the fractal aggregate, ξ is the upper cutoff (fractal correlation length and is defined as the maximum length up to which fractal correlation exists). Estimated size distributions of the primary particles at different sintering temperatures are depicted in figure 2.

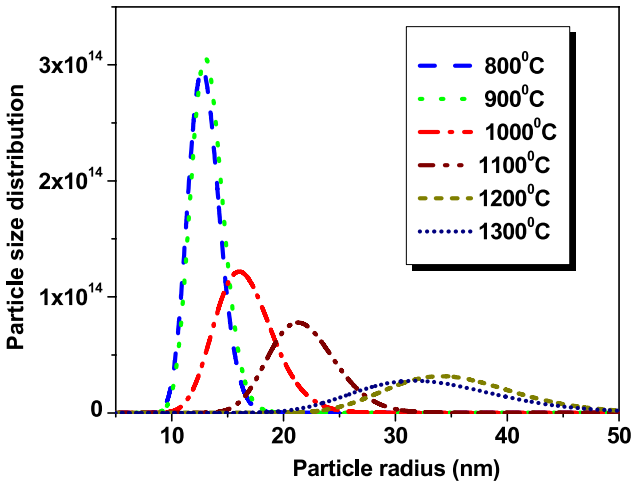

Figure 2. The primary particle size distribution with increasing sintering temperature. It is found that the average particle size increases with temperature.

4. Computer simulation

To interpret the experimental observations, a computer simulation has been carried out. In last two decades, various computer models have been developed to simulate random fractal objects originating from the agglomeration of the smaller particles. Some of these models are diffusion limited aggregation (DLA) [52], cluster–cluster aggregation (CCA) [53], tunable dimension cluster–cluster aggregation (tCCA) [54, 55] and reaction limited cluster–cluster aggregation (RLCCA) [56].

It is observed from scattering experiments that YAG nano-ceramic possesses a fractal type of aggregates. The fractal dimension D_{F} has been found to be approximately 2.3 ± 0.2, indicating a diffusion limited aggregate type of fractal morphology of the aggregates. The DLA model is one of the simplest models of this kind. Such a fractal cluster can develop during the diffusion control growth and the choice of DLA like fractal cluster is physically motivated. Due to the computational complexity, the present simulation has been restricted to a two dimensional DLA cluster as the starting aggregate model. In the present simulation, a DLA cluster consisting of 10 000 particles is generated on a square lattice. At the beginning of the simulation, the mass and radius of a particle have been taken to be 1.0 unit and 0.5 units, respectively.

We know that the particles in fractal aggregates are connected by attractive forces such as van der Waals or other molecular forces resulting in covalent bonding. The bonds between the particles represent an energy barrier that prevents rearrangement. A minimum energy is required to overcome such an energy barrier. It is important to note that for restructuring of the aggregate, it is not necessary to break the bonds completely. Therefore, it is expected that the activation energy E_{a} for rearrangement of the aggregate is lower than the bond energy E_{b} [20]. It is interesting to mention that the driving force for mass transport during sintering is the high surface energy of the aggregate of fine

particles. Diffusion transports matter along free surfaces and volumes of particles along grain boundaries between them; there is also transportation of matter mediated through a vapour phase around them. The diffusion coefficients, for different processes involved, are different from each other. A numerical simulation of sintering process is complex as various diffusion processes are relevant at different stages of sintering, albeit, we attempted a model for simulation to explain the experimental observations. In the present simulation, an effective diffusion coefficient has been defined to account for all the diffusion transport mechanisms. A localized sintering model has been adopted [39] to simulate the structural evolution of fractal clusters as a function of sintering temperature. This model is based on the experimentally observed phenomenon that sintering starts with the merging of neighbouring particles that are in contact in the aggregate [29]. It is interesting to note that the model of local group merge sintering involves the diffusion of matter locally and the detailed kinetics of the sintering is ignored. The present model also deals with mass transport from higher to lower curvature in an indirect fashion because the curvature of the merged particle is smaller than the curvatures of the individual particles before merging.

The diffusion length in a sintering process is defined as

$$\sqrt{\langle r^2(t)\rangle} = \sqrt{D_{\text{eff}} t}, \tag{3}$$

where D_{eff} is the effective diffusion coefficient and t is time. In the present model, diffusion of particles occurs locally. Thus, the sintering distance Δ_s is assumed to be equal to the diffusion length. From the Arrhenius equation, the diffusion coefficient D_{eff} is related to temperature T,

$$D_{\text{eff}} = D_0 \exp(-E_a/kT), \tag{4}$$

where D_0 is a constant. Here, the activation energy has been assumed to be independent of temperature for a small temperature variation. From equations (3) and (4), a relation between Δ_s and sintering temperature at a fixed time may be derived as

$$T = \frac{C_1}{C_2 + \log(1/\Delta_s^2)} \tag{5}$$

where C_1 $(=E_a/k)$ and C_2 $(=\log(D_0 t))$ are temperature independent constants. From equation (5), it is evident that Δ_s increases with increasing sintering temperature.

It is interesting to note that the sintering distance Δ_s is not only a function of the temperature but also depends on the size of the particle formed by the merging of smaller particles. In the present model, an Ostwald-ripening type of evolution of fractal aggregates under conservative conditions is adopted. It means that the larger the particle size in the cluster, the larger is Δ_s. A larger particle would grow at the expense of the smaller ones keeping the mass conserved.

Local group merge restructuring is carried out according to the following algorithm. First, any particle in the cluster is chosen randomly. The neighbouring particles are calculated according to some fixed sintering distance Δ_s then grouped and merged to form a new particle. The mass of this bigger particle will be the sum of the masses of all the merging particles and the radius is calculated in accordance with the mass conservation of the system. The centre of the new primary particle will be situated at the centre of mass of the merged particles. An off-lattice model is used to displace the new primary particles, formed by merging of the smaller particles, towards the centre of mass of the DLA aggregate with the condition that all neighbouring particles remain in contact. Then another random particle is chosen for the same Δ_s and the above mentioned process is reiterated. This process is carried out repeatedly while we can find some neighbours for same Δ_s.

Simulation steps are performed for increasing Δ_s by using the above algorithm as sintering temperature increases. The evolution of fractal cluster with Δ_s is shown in figure 3. The fractal dimension of the cluster before and after the sintering restructuring can be calculated by the power law relationship between mass and radius, $M \propto R_F^D$, where R is the radius of the searching circle assuming the centre of mass of the cluster as the origin. The fractal dimension of the initial DLA cluster has been estimated in figure 4. Similarly, the fractal dimension of the modified DLA clusters have also been estimated. It is interesting to note that, for a fixed Δ_s, the chosen random particle in the DLA cluster may have different numbers of neighbours, accordingly, after the first step of the simulation, the primary particle size will be polydisperse in nature. The evolution of size distribution of primary particles with Δ_s is shown in figure 5.

The lower cutoffs of the fractal aggregate for each Δ_s have been estimated by taking an average of the size distribution. The upper cutoff is assumed as the radius of gyration R_g of the fractal cluster, $R_g^2 = \sum_i m_i r_i^2 / \sum_i m_i$, where m_i is the mass of the ith particle in the cluster, r_i is the distance of the ith particle from the centre of mass of cluster. The evolution of the cutoffs of the fractal aggregate are shown in figure 6.

5. Results and discussion

From figure 1, scattering profiles of YAG nano-ceramic indicate the fractal morphology of aggregates at all sintering temperatures under study. However the extent of the linear region of the profiles in the log–log plot decreases with increasing sintering temperature, exhibiting modification in the upper and lower cutoffs of the fractal aggregate. From figure 3, the evolution of the DLA cluster is shown for different Δ_s vis-à-vis different simulation sintering temperature. Initially, a DLA aggregate is not very compact and many sites, in particular edge sites, of a cluster have relatively fewer neighbours, leading to a higher surface area of the cluster. Sintering provides the required activation energy to the atoms for diffusion. Diffusion of the atoms plays an important role in deciding the morphological change during sintering. Two types of diffusion mechanism are possible. In one case, the diffusion occurs in small steps, i.e. the mobility of the cluster atoms is lower, and in the second case, diffusion occurs over an extended zone in large steps with a higher mobility of the cluster atoms. Depending upon the type of diffusion process, the morphology of the cluster gets modified accordingly. In the case of the present model, small step diffusion dominates over extended zone diffusion. This process leads to local smoothening of the aggregate branches by keeping the overall

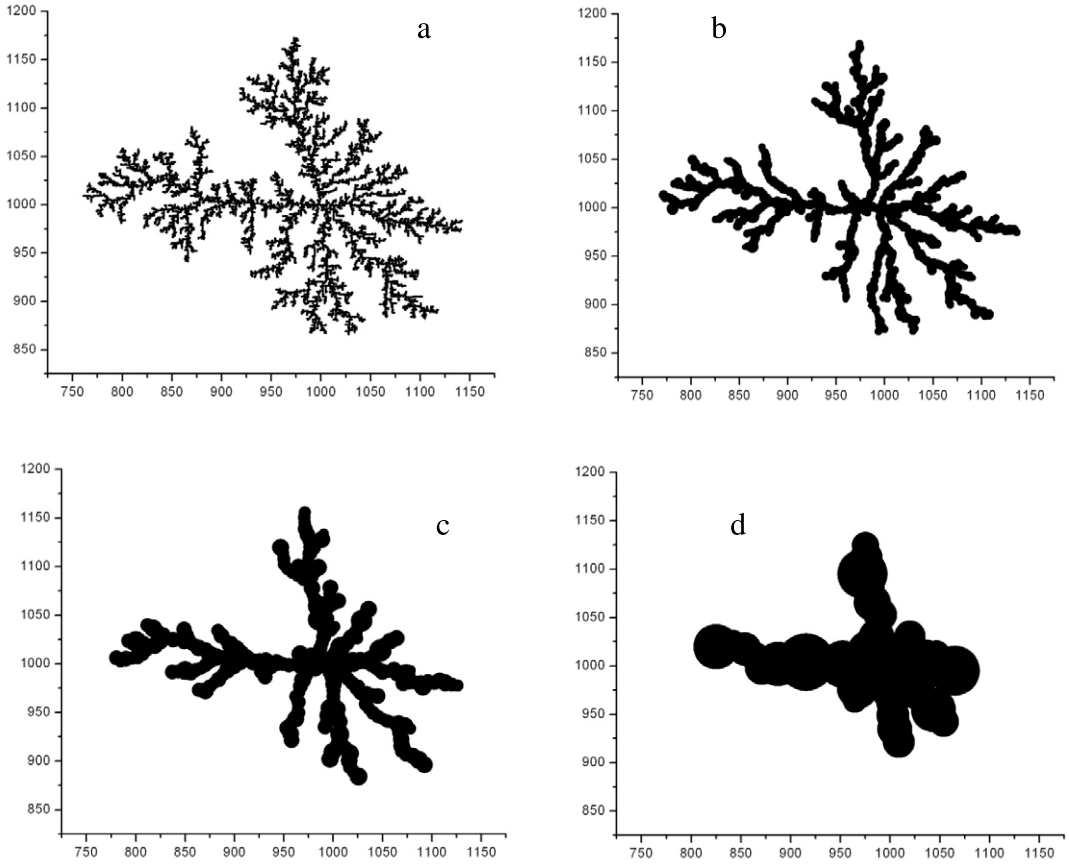

Figure 3. Evolution of the DLA clusters with different Δ_s. (a) Initial 2D DLA. (b) Modified DLA for $\Delta_s = 10$. (c) Modified DLA for $\Delta_s = 30$. (d) Modified DLA for $\Delta_s = 150$.

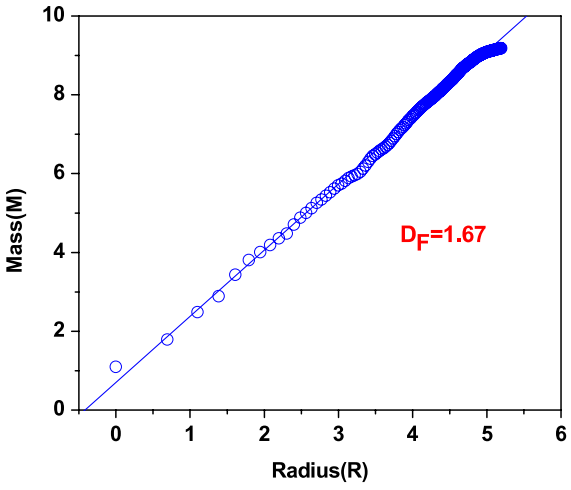

Figure 4. Estimated fractal dimension of the initial DLA cluster from the power law relationship in logarithm.

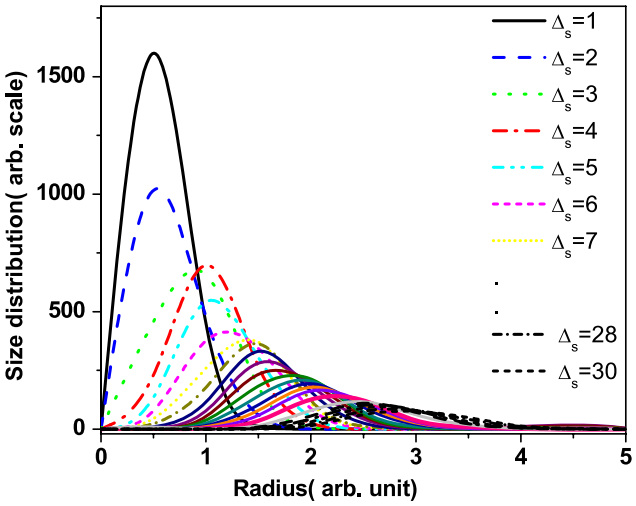

Figure 5. Evolution of the primary particle size distribution as function of $\Delta_s(T)$.

cluster morphology unaltered. However, at significantly high temperature, even the low resolution morphology gets modified, as is evident from figure 3. Interestingly, it has been observed that variation of the lower cutoff with sintering temperature may be represented as a power law with an exponent 1/2, i.e. $R_{av} \propto \Delta_s^{1/2}$. Similarly, the variation of the upper cutoff with temperature may be represented as a power law with an exponent 1/3, i.e. $\xi \sim C_1 - C_2\Delta_s^{1/3}$, where C_1 and C_2 are positive constants. It is worth mentioning that, although diffusion mechanisms may dominate at different temperatures, the present sintering model could still explain the variation of cutoffs by power law with a single exponent in the present range of the sintering temperature.

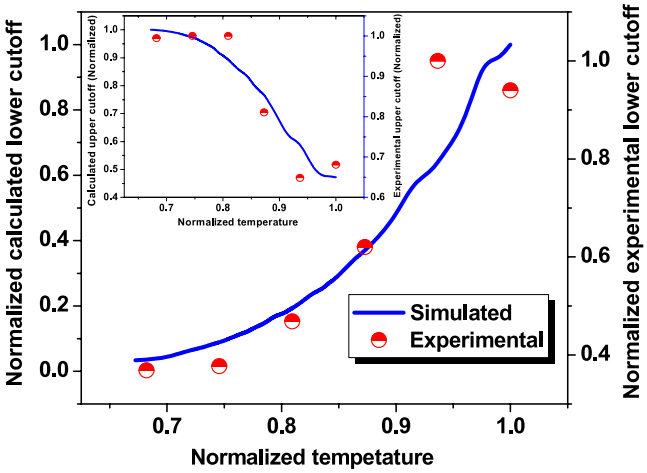

Figure 6. Computed lower cutoff from simulation and the observed lower cutoff from SANS at different temperatures are depicted. The inset shows computed upper cutoff from simulation and observed upper cutoff from SANS.

The experimental and simulated fractal cutoffs at different sintering temperatures (normalized scale) are depicted in figure 6. It is evident that the variation of experimental and calculated cutoff lengths corroborate each other within experimental error bars. In the real situation, the sintering process involves different mass transport mechanisms at different stages of sintering. In the present simulation, the mechanism for mass transport has been assumed to be the same for all temperature regimes. This assumption could be one of the reasons for the small deviation in the simulated and experimental cutoffs of fractal aggregates. Furthermore, it should also be noted that nano-ceramics possess high surface area as compared to their bulk counterpart. The activation energy, required for diffusion, is lower in nano-ceramics vis-a-vis to their bulk counterpart. Thus, sinterability of the nano-ceramics is larger as compared to the bulk ceramics [57]. This may lead to some deviation in the experimental and simulated results. In the present simulation, the evolution of the particle size distribution with temperature estimated from experiments corroborates that obtained from the simulation. The initial DLA cluster consists of monodisperse particles, the polydispersity in size distribution of the particles creeps in as sintering proceeds.

6. Conclusions

Scattering experiments reveal that YAG nano-ceramics are made of fractal aggregates. The cutoff lengths vary with sintering temperature while the fractal dimension of the cluster remains same. A local group merge sintering model has been adopted to modify the 2D DLA cluster and explain the experimental observations. The evolution of the primary particle size distribution is also examined by numerical simulation. The results of numerical simulations corroborate the experimental observations. Thermal relaxation of a fractal aggregate to its equilibrium shape is an exterior surface modifying process of a self-similar structure. Since the global configuration of the aggregate remains intact, except in the last stage of relaxation, the change of the fractal dimension is disregarded in the present simulation. The main effect of thermal relaxation under annealing of the YAG fractal cluster is the coarsening of the fractal structure keeping the fractal dimension invariant. Coarsening of the fractal aggregate indicates the nature of binding of the primary particle within the aggregate. The particles are binding each other strongly, i.e. mobility of the atoms is less, but at elevated temperature they can move locally to the branches of the fractal clusters. In short, the present model of local sintering is a suitable model to understand such observations.

References

[1] Rayleigh J W S 1879 *Proc. London Math. Soc.* **10** 4
[2] Chandrasekhar S 1961 *Hydrodynamics and Hydrodynamic Stability* (New York: Oxford University Press)
[3] Eggers J 1997 *Rev. Mod. Phys.* **69** 865
[4] Mullins W W 1957 *J. Appl. Phys.* **28** 333
[5] Nichols F A and Mullins W W 1965 *J. Appl. Phys.* **36** 1826
[6] Nichols F A and Mullins W W 1965 *Trans. Metall. Soc. AIME* **233** 1840
[7] Thomspson D 1961 *On the Growth and Form* (Cambridge: Cambridge University Press)
[8] Langer J S 1980 *Rev. Mod. Phys.* **52** 1
[9] Moseler M and Landman U 2000 *Science* **289** 1165
[10] Mullins W W and Sekerka R F 1963 *J. Appl. Phys.* **34** 323
[11] Mandelbrot B B 1983 *The Fractal Geometry of Nature* (New York: Freeman)
[12] Bunde A and Havlin S (ed) 1991 *Fractals and Disordered Systems* (New York: Springer)
[13] Avnir D 1989 *The Fractal Approach to Heterogeneous Chemistry* (New York: Wiley)
[14] Hwang R Q, Schröder J, Günther C and Behm R J 1991 *Phys. Rev. Lett.* **67** 3279
[15] Sempere R, Bourret D, Woignier T, Phalippou J and Jullien R 1993 *Phys. Rev. Lett.* **71** 3307
[16] Irisawa T, Uwaha M and Saito Y 1995 *Europhys. Lett.* **30** 139
[17] Olivi-Tran N, Thouy R and Jullien R 1996 *J. Physique* I **6** 557
[18] Thouy R, Olivi-Tran N and Jullien R 1997 *Phys. Rev.* B **56** 5321
[19] Conti M, Meerson B and Sasorov P V 1998 *Phys. Rev. Lett.* **80** 4693
[20] Weber A P and Friedlander S K 1997 *J. Aerosol Sci.* **28** 179
[21] Schmidt-Ott A 1988 *J. Aerosol Sci.* **19** 553
[22] Huang P, Turpin B J, Pipho M J, Kittelson D B and McMurry P H 1994 *J. Aerosol Sci.* **25** 447
[23] Jullien R and Meakin P 1989 *J. Colloid Interface Sci.* **127** 265
[24] Bre'chignac C, Cahuzac Ph, Carlier F, Colliex C, Roux J Le, Masson A, Yoon B and Landman U 2002 *Phys. Rev. Lett.* **88** 196103
[25] Hwang R Q, Schröder J, Günther C and Behm R J 1991 *Phys. Rev. Lett.* **67** 3279
[26] Sharon E, Moore M G, McCormick W D and Swinney H L 2003 *Phys. Rev. Lett.* **91** 205504
[27] Conti M, Lipshtat A and Meerson B 2004 *Phys. Rev.* E **69** 031406
[28] Flagan R C and Lunden M M 1995 *Mater. Sci. Eng.* A **204** 113
[29] Lehtinen E J, Windeler R S and Friedlander S K 1996 *J. Aerosol Sci.* **27** 883
[30] Schaefer D W, Olivier B J, Ashley C, Beaucage G, Richter D, Farago B, Frick B and Fischer D A 1994 *J. Non-Cryst. Solids* **172/173** 647
[31] Olivi-Tran N, Jullien R and Cohen-Solal G W 1995 *Europhys. Lett.* **30** 393

[32] Olivi-Tran N and Jullien R 1995 *Phys. Rev.* B **52** 258
[33] Olivi-Tran N and Jullien R 1997 *J. Sol–Gel Sci. Technol.* **8** 813
[34] Mazumder S, Sen D, Patra A K, Khadilkar S A, Cursetji R M, Loidl R, Baron M and Rauch H 2004 *Phys. Rev. Lett.* **93** 255704
[35] Mazumder S, Sen D, Patra A K, Khadilkar S A, Cursetji R M, Loidl R, Baron M and Rauch H 2005 *Phys. Rev.* B **72** 224208
[36] Mazumder S, Loidl R and Rauch H 2007 *Phys. Rev.* B **76** 064205
[37] Sen D, Mahata T, Patra A K, Mazumder S and Sharma B P 2004 *J. Phys.: Condens. Matter* **16** 6229
[38] Sen D, Mazumder S and Bahadur J 2009 *Phys. Rev.* B **79** 134207
[39] Yang G and Biswas P 1999 *J. Colloid Interface Sci.* **211** 142
[40] Koch W and Friedlander S K 1990 *J. Colloid Interface Sci.* **140** 419
[41] Kobata A, Kusakabe K and Morooka S 1991 *J. AIChE* **37** 347
[42] Ramanathan S, Roy S K and Ravindran P V 2000 *Trans. Indian Ceram. Soc.* **59** 12
[43] Guinier A, Fournet G, Walker B C and Yudowith L K 1955 *Small Angle Scattering of X-Rays* (New York: Wiley) p 167
[44a] Glatter O and Kratky O 1982 *Small Angle X-Ray Scattering* (London: Academic)
[44b] Kingery W D, Bowden H K and Uhlmann D R 1976 *Introduction to Ceramics* (*Wiley Series on the Science and Technology of the Materials*) 2nd edn (New York: Wiley) p 1032
[45] Sen D, Bahadur J, Mazumder S, Bedekar V and Tyagi A K 2008 *J. Phys.: Condens. Matter* **20** 035103
[46] Bahadur J, Sen D, Mazumder S, Shukla R and Tyagi A K 2008 *J. Phys.: Condens. Matter* **20** 345201
[47] Mazumder S, Sen D, Sarvanan T and Vijayraghavan P R 2001 *J. Neutron Res.* **9** 39
[48] Lake J A 1967 *J. Appl. Crystallogr.* **23** 191
[49] Maul J, Marosits E, Sudek Ch, Berg T and Ott U 2005 *Phys. Rev.* B **72** 245401
[50] Teixeira J 1988 *J. Appl. Crystallogr.* **21** 781
[51] Freltoft T, Jems J K and Sinha S K 1986 *Phys. Rev.* B **33** 269
[52] Witten T A and Sander L M 1981 *Phys. Rev. Lett.* **47** 1400
[53] Meakin P 1983 *Phys. Rev. Lett.* **51** 1119
[54] Thouy R and Jullien R 1994 *J. Phys. A: Math. Gen.* **27** 2953
[55] Thouy R and Jullien R 1996 *J. Physique* **16** 1365
[56] Meakin P and Family F 1988 *Phys. Rev.* A **38** 2110
[57] Campbell C T, Parker S C and Starr D E 2002 *Science* **298** 811